ISSN 1674-1056
http://cpb.iphy.ac.cn
http://iopscience.iop.org/cpb
中国物理 B
Chinese Physics
中国物理
Chinese Physics B

Electro-optomechanical switch via tunable bistability and four-wave mixing

Kamran Ullah

Citation: Chin. Phys. B . 2019, 28(11): 114209 . **doi:** 10.1088/1674-1056/ab4580
Journal homepage: http://cpb.iphy.ac.cn; http://iopscience.iop.org/cpb

What follows is a list of articles you may be interested in

Silicon nanophotonics for on-chip light manipulation

Jingshu Guo(郭敬书), Daoxin Dai(戴道锌)

Chin. Phys. B . 2018, 27(10): 104208 . **doi:** 10.1088/1674-1056/27/10/104208

Controllable optical bistability in a three-mode optomechanical system with a membrane resonator

Jiakai Yan(闫甲楷), Xiaofei Zhu(朱小霏), Bin Chen(陈彬)

Chin. Phys. B . 2018, 27(7): 074214 . **doi:** 10.1088/1674-1056/27/7/074214

Controllable double electromagnetically induced transparency in a closed four-level-loop cavity–atom system

Miao-Di Guo(郭苗迪), Xue-Mei Su(苏雪梅)

Chin. Phys. B . 2017, 26(7): 074207 . **doi:** 10.1088/1674-1056/26/7/074207

Vacuum induced transparency and slow light phenomena in a two-level atomic ensemble controlled by a cavity

Guo Yu-Jie, Nie Wen-Jie

Chin. Phys. B . 2015, 24(9): 094205 . **doi:** 10.1088/1674-1056/24/9/094205

Single photon transport properties in coupled cavity arrays nonlocally coupled to a two-level atom in the presence of dissipation

Hai Lian, Tan Lei, Feng Jin-Shan, Xu Wen-Bin, Wang Bin

Chin. Phys. B . 2014, 23(2): 024202 . **doi:** 10.1088/1674-1056/23/2/024202

Electro-optomechanical switch via tunable bistability and four-wave mixing

Kamran Ullah†

Department of Physics, Quaid-i-Azam University, Islamabad 45320, *Pakistan*

(Received 30 May 2019; revised manuscript received 14 July 2019; published online 1 November 2019)

We investigate the tunable bistable behavior of a hybrid nano-electro-optomechanical system (NEOMS) composed of S-shaped in the presence of two-level atoms, trapped inside a Fabry–Pérot cavity, and driven by a strong driving field and a weak probe field. The bistable behavior of the steady-state photon number and the mechanical steady-state positions are discussed. Further, we tune bistability by tuning all the coupling frequencies involved in the system and amplitude of the driving field. The present study provides the possibility of realization of a controllable optical switch depending on atom-field coupling, optomechanical coupling, electrostatic Coulomb coupling, and threshold power. In addition, we discuss that the non-linear effect of the hybrid NEOMS generates the four-wave mixing (FWM) process. Moreover, we show that the FWM process can be suppressed by the atom-field detuning and cavity-field detuning, which exhibits low photon transmission.

Keywords: nano-electro-optomechanics, nano-resonators, two-level atom, optical switch, optical bistability, four-wave mixing

PACS: 42.79.Ta **DOI:** 10.1088/1674-1056/ab4580

1. Introduction

Nowadays in optomechanics, the micro/nano-mechanical resonators (NMRs) provide a suitable platform to study quantum coherence in a macroscopic system in various ways. The combination of a micro/nano-mechanical resonator with other miniatures like electron spin,[1] mechanical membrane,[2,3] nitrogen vacancy (NV),[4] optical cavities,[5–7] and Bose–Einstein condensate (BEC),[8,9] has a pathway in manufacturing hybrid systems.[10–12] The hybrid systems have a lot of aspiring applications, such as, dipole blockade approach,[13,14] and simulating many-body quantum systems,[15] respectively. In an optomechanical system, the interaction of laser light with a moving mirror generates the radiation pressure force[16,17] which depends on the displacement of the movable mirror. In the presence of strong driving power, the field inside the cavity is sufficiently strong to trip nonlinear behavior of the system. So far, the investigation of atom-assisted optomechanics composed of movable cavities as well as ultra-cold atoms leads to various configurations by quantum cavity field and classical pump field.[18–20] Many important works have been done in this interesting field like ground-state cooling of mechanical resonators,[21–24] electromagnetically induced transparency (EIT),[25–27] quantum dot,[28] quantum squeezing,[29–31] qubits,[32] and atomic ensemble.[33–35]

Optical bistability arises due to the nonlinear characteristics of the optical field, and therefore, exhibits hysteresis.[36] In simple optomechanical system, the optical bistability with Kerr effect was studied in Refs. [37] and [38], and in quantum degenerate Fermi gas[39] on the one hand. While in hybrid optomechanical systems composed of ultra-cold trapped atoms such as BEC,[40–43] two-level atoms[44] on the other hand. Besides, the optical bistability has also been discussed in double cavity systems[45,46] as well as in a composite photonic molecule cavity optomechanical system consisting of two whispering gallery mode microcavities.[47] Optical bistability has many practical applications in the field of nonlinear optics, for example, signal processing,[48] all-optical switching,[49] all-optical transistors,[50] and all-optical sensing elements.[51]

Like optical bistability, the four-wave mixing (FWM) intensity process is also a nonlinear effect of the quantum-optical field based on quantum coherence and quantum interference which is frequently studied in the nonlinear optics. Consequently, we have a large number of different applications of quantum coherence and interferences in optomechanical systems, names of few, frequency conversion,[52] the observation of entanglement,[53] stopped light,[54] and fast light.[55] The experimental aspect of the non-degenerate FWM in a three-level system was studied in Ref. [56]. After that, the enhanced FWM process in ultra-slow pump waves was discussed in Ref. [57]. Recently, it has been theoretically observed that the FWM can be instigated in oscillatory tunneling antisymmetric quantum wells[58] which is analogous to electromagnetically induced transparency.[59] More recently, the FWM process in optomechanical system has been studied in Ref. [60]. Moreover, the quantum mechanical behavior of the FWM was not only explained in BEC[61] but also discussed in quantum degenerate Fermi gas.[62,63] In addition, the

†Corresponding author. E-mail: kamran@phys.qau.edu.pk

© 2019 Chinese Physical Society and IOP Publishing Ltd

controllable FWM has not only been studied in a two-mode optomechanical system[64] but also discussed in a composite photonic-molecule cavity optomechanical system.[65]

In the present work, we suggest a hybrid nano-electro-optomechanical system (NEOMS) for detail analysis of bistability and FWM intensity process. The suggested NEOMS comprises two charged nano-mechanical resonators NMR_1 and NMR_2 that are connected to an external bias gate V_1 $(-V_2)$. The NMR_1 (NMR_2) is charged through V_1 $(-V_2)$ and produces Coulomb coupling between NMR_1 and NMR_2. The optical cavity is loaded by N number of two-level atoms. In this work, we show that the hybrid NEOMS can be coupled with two-level atoms through the cavity field of the device. Experimental progress is made on the coupling between mechanical resonators and two-level system, e.g., superconducting qubits,[66] cascaded optomechanical devices,[67–69] Ising model,[70] and electro-optomechanical system.[71–74]

In this work: (i) we present that our numerical study is focused on resonant interactions between the low-frequency of NMR_1 (NMR_2) and two-level atom; (ii) the obtained results provide the threshold driving field for the bistable region that can be controlled by N and cavity field, respectively; (iii) keep in mind that the previous studies on bistability are composed of simple optomechanical systems where the bistability is a function of optomechanical coupling or a Kerr medium.[37,38] In case of hybrid optomechanical systems composed of ultracold atoms,[40–43] the bistability can be controlled by two coupling frequencies, i.e., atom-field coupling and optomechanical coupling. These systems work in certain parametric regime but has no external controllable source. Therefore, we consider a hybrid optomechanical system in which the optical bistability is not only controlled by new systematic parameters such as frequency ω_1 (ω_2) and mass m_1 (m_2) of the resonator, but also controlled electrostatically through Coulomb coupling g_c via external bias gate V_1 $(-V_2)$. By doing so, we not only control the Coulomb coupling between NMR_1 and NMR_2 but also control the mirror field coupling.

The rest of the paper is as follows. In Section 2, we describe the basic theory of the proposed model and derive the Heisenberg Langevin equations of motion, respectively. In Section 3, we discuss the steady-state solution of the system and analyze the bistable behavior of the steady-state photon number and the steady-state position of NMR_1 (NMR_2). In Section 4, we study the nonlinear behavior of the system in term of four-wave mixing process. In Section 5, we present the conclusion.

2. Theoretical model and formalism

The suggested model comprises an ensemble of two-level atoms inside a Fabry–Pérot cavity of length L, a fixed mirror, and end moving coupled charged nano-mechanical resonators NMR_1 and NMR_2 as shown in Fig. 1. The NMR_1 is not only coupled with cavity field and sharing optomechanical coupling g_0 but also coupled to NMR_2 electrostatically via Coulomb coupling g_c. The cavity mode is driven by a strong laser field and a weak field of amplitudes E_L and ε_p, respectively. The charge on NMR_1 is $e_1 = C_1V_1$ due to V_1, whereas the charge on NMR_2 is $e_2 = -C_2V_2$ due to $-V_2$; here, C_1 (C_2) is capacitor bank. In addition, the Coulomb coupling g_c is tuned by bias gate V_1 $(-V_2)$. We consider the Jayen's cumming type interaction[75] to the cavity field, and the Hamiltonian of the systems can be read as

$$H = H_0 + H_I, \tag{1}$$

where H_0 and H_I represent the free Hamiltonian and interaction Hamiltonian of the system, respectively. The free Hamiltonian is

$$\begin{aligned} H_0 &= \hbar\omega_c\hat{a}^\dagger\hat{c} + \frac{1}{2}\hbar\omega_a\sum_{n=1}^{N}\hat{\sigma}_z^n + \sum_{j=1}^{2}\left(\frac{\hat{p}_j^2}{2m_j} + \frac{1}{2}m_j\omega_j^2\hat{q}_j^2\right) \\ &\quad + i\hbar E_L(\hat{c}^\dagger e^{-i\omega_L t} - \text{H.c.}) + i\hbar(\hat{c}^\dagger\varepsilon_p e^{-i\omega_p t} - \text{H.c.}). \end{aligned} \tag{2}$$

And the interaction Hamiltonian is

$$H_I = \hbar g_a\sum_{n=1}^{N}(\hat{\sigma}_+^n\hat{c} + \hat{\sigma}_-^n\hat{c}^\dagger) - \hbar g_0\hat{c}^\dagger\hat{c}\hat{q}_1 + \hbar g_c\hat{q}_1\hat{q}_2, \tag{3}$$

where in Eq. (2), $c^\dagger$ (c) is the creation (annihilation) operator of the cavity field, $E_L = \sqrt{\frac{2\wp_1\kappa}{\hbar\omega_L}}$, and $\varepsilon_p = \sqrt{\frac{2\wp_p\kappa}{\hbar\omega_p}}$. Here, $\wp_1$ and $\wp_p$ correspond to laser and probe field powers. The term $\hat{\sigma}_z$ is the atomic transition operator between the two levels and oscillates with frequency ω_a. The third term of Eq. (2) represents the energy of NMR_1 (NMR_2), and m_j and ω_j are the effective mass and mechanical frequency of the resonators. Moreover, $\hat{q}_j$ ($\hat{p}_j$) is the position (momentum) operator for NMR_j with $j = 1, 2$. In Eq. (3), the first term represents the atom-field interaction whereas the second term represents the mirror field interaction and expressed as $g_0 = \hbar\omega_c/L$. Moreover, the last term belongs to Coulomb interaction between NMR_1 and NMR_2 and related to $g_c = -\frac{C_1V_1C_2V_2}{2\pi\hbar\varepsilon_0 r_0^3} = \frac{e_1e_2}{2\pi\hbar\varepsilon_0 r_0^3}$,[72,76] where r_0 is the relax distance between NMR_1 and NMR_2. Here, σ_+^n and $\hat{\sigma}_-^n$ are respectively the spin matrices that satisfy the commutation relation $[\hat{\sigma}_\pm^n, \hat{\sigma}_\mp^n] = \pm\hat{\sigma}_z^n$ and $[\hat{\sigma}_z^n, \hat{\sigma}_\pm^n] = \pm 2\hat{\sigma}_\pm^n$. Here, we introduce new bosonic annihilation (creation) operator such as $\hat{b} = \frac{\sum_{n=1}^{N}\hat{\sigma}_-^n}{\sqrt{\sum_{n=1}^{N}|\langle\hat{\sigma}_z^n\rangle|}}$, $\hat{b}^\dagger = \frac{\sum_{n=1}^{N}\hat{\sigma}_+^n}{\sqrt{\sum_{n=1}^{N}|\langle\hat{\sigma}_z^n\rangle|}}$, with bosonic commutation relations $[\hat{b}, \hat{b}^\dagger] = 1$ and $\sum_{n=1}^{N}\hat{\sigma}_z^n = 2\hat{b}^\dagger\hat{b} - N$.[77] At ground state, atoms satisfy the relation $\sum_{n=1}^{N}\hat{\sigma}_z^n = \sum_{n=1}^{N}\langle\hat{\sigma}_z^n\rangle = -N$. By rotating frame according to laser frequency ω_L, the Hamiltonian of the system is modified as

$$\begin{aligned} H &= \hbar\Delta_c\hat{c}^\dagger\hat{c} + \hbar\Delta_a\hat{b}^\dagger\hat{b} + \sum_{j=1}^{2}\left(\frac{\hat{p}_j^2}{2m_j} + \frac{1}{2}m_j\omega_j^2\hat{q}_j^2\right) \\ &\quad - \hbar g_0\hat{c}^\dagger\hat{c}\hat{q}_1 + \hbar g_a\sqrt{N}(\hat{b}^\dagger\hat{c} + \hat{b}\hat{c}^\dagger) + \hbar g_c\hat{q}_1\hat{q}_2 \end{aligned}$$

$$+\mathrm{i}\hbar E_{\mathrm{L}}(\hat{c}^{\dagger}-\hat{c})+\mathrm{i}\hbar(\hat{c}^{\dagger}\varepsilon_{\mathrm{p}}\mathrm{e}^{-\mathrm{i}\delta t}-\hat{c}\varepsilon_{\mathrm{p}}^{\star}\mathrm{e}^{\mathrm{i}\delta t}). \tag{4}$$

In Eq. (4), $\Delta_{\mathrm{c}}=\omega_{\mathrm{c}}-\omega_{\mathrm{L}}$ is the cavity detuning whereas $\Delta_{\mathrm{a}}=\omega_{\mathrm{a}}-\omega_{\mathrm{L}}$ represents the atom-field detuning corresponding to laser frequency. Moreover, δ is the probe field detuning corresponding to $\omega_{\mathrm{p}}-\omega_{\mathrm{L}}$.

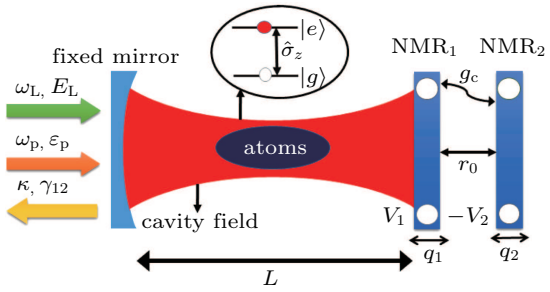


Fig. 1. The demonstration of suggested NEOMS composed of N number of two-level atoms follows by moving-end two charged nanomechanical resonators NMR$_1$ and NMR$_2$. The first mirror is coupled to the cavity field and MMR$_2$, respectively. The NMR$_1$ (NMR$_2$) is charged by a bias voltage V_1 ($-V_2$), where g_{c} is the Coulomb coupling and r_0 is the relax position of NMR$_1$ (NMR$_2$). Here, q_1 (q_2) represents the small displacement of NMR$_1$ (NMR$_2$) from their relax position. Moreover, L is the cavity length and $\hat{\sigma}_z$ corresponds to transition operator between the two levels.

Here, we study the steady-state solution of the system, therefore, we introduce the mean value approximation where all the noise terms have been vanished. By considering all fluctuations and decay terms at the mean field approximation, i.e., $\langle\hat{A}^{\dagger}\hat{A}\rangle=\langle\hat{A}^{\dagger}\rangle\langle\hat{A}\rangle$,[25] the mean value equations of Eq. (4) can be found as

$$\begin{aligned}
&\langle\dot{\hat{q}}_j\rangle=\frac{\langle\hat{p}_j\rangle}{m_j},\\
&\langle\dot{\hat{p}}_1\rangle=-m_1\omega_1^2\langle\hat{q}_1\rangle+g_0\langle\hat{c}^{\dagger}\rangle\langle\hat{c}\rangle-g_{\mathrm{c}}\langle\hat{q_2}\rangle-\gamma_1\langle\hat{p}_1\rangle,\\
&\langle\dot{\hat{p}}_2\rangle=-m_2\omega_2^2\langle\hat{q}_2\rangle-g_{\mathrm{c}}\langle\hat{q}_1\rangle-\gamma_2\langle\hat{p}_2\rangle,\\
&\langle\dot{\hat{c}}\rangle=-(\kappa+\mathrm{i}\Delta_{\mathrm{c}})\langle\hat{c}\rangle+\mathrm{i}g_0\langle\hat{c}\rangle\langle\hat{q}_1\rangle-\mathrm{i}g\langle\hat{b}\rangle+E_{\mathrm{L}}+\varepsilon_{\mathrm{p}}\mathrm{e}^{-\mathrm{i}\delta t},\\
&\langle\dot{\hat{b}}\rangle=-(\gamma_{\mathrm{a}}+\mathrm{i}\Delta_{\mathrm{a}})\langle\hat{b}\rangle-\mathrm{i}g\langle\hat{c}\rangle.
\end{aligned}\tag{5}$$

Here, γ_1 (γ_2) is the decay term corresponding to NMR$_1$ (NMR$_2$), whereas γ_{a} represents the decay of the atomic oscillation. We take $\hbar=1$, and $g=g_{\mathrm{a}}\sqrt{N}$ represents the total coupling strength between atoms and cavity field which depends on the number of atoms. Moreover, κ is the decay term of the cavity field. Further, equation (5) represents a set of non-linear equations corresponding to the mean values. To derive the steady-state solution, we introduce new operators as Ref. [78]. Therefore, $\langle\hat{A}\rangle=A_{\mathrm{s}}+\hat{A}_{-}\mathrm{e}^{-\mathrm{i}\delta t}+\hat{A}_{+}\mathrm{e}^{\mathrm{i}\delta t}$. Here, A_{s} represents the steady-state of c_{s}, $q_{i\mathrm{s}}$, $p_{i\mathrm{s}}$ ($i=1,2$), while $\hat{A}_{\pm}$ is considered as perturbations with frequencies ω_{L}, ω_{p}, $2\omega_{\mathrm{L}}-\omega_{\mathrm{p}}$, respectively. The zero order solutions for the steady-state operator can be written as

$$p_{i\mathrm{s}}=0,\quad q_{1\mathrm{s}}=\frac{g_0|c_{\mathrm{s}}|^2}{m_1\omega_1^2-\frac{g_{\mathrm{c}}^2}{m_2\omega_2^2}},$$

$$\begin{aligned}
&q_{2\mathrm{s}}=\frac{-g_{\mathrm{c}}q_{1\mathrm{s}}}{m_2\omega_2^2},\quad c_{\mathrm{s}}=\frac{E_{\mathrm{L}}}{\kappa+\mathrm{i}\Delta+\frac{g^2}{\gamma_{\mathrm{a}}+\mathrm{i}\Delta_{\mathrm{a}}}},\\
&\Delta=\Delta_{\mathrm{c}}-g_0q_{1\mathrm{s}}.
\end{aligned}\tag{6}$$

3. Tunable bistability

We use the conventional approach of the optomechanical system to perform the bistable behavior of the steady-state photon number and mechanical steady-state position of the resonators. The set of steady-state equations (Eq. (6)) can be written as

$$|c_{\mathrm{s}}|^2=\left|\frac{E_{\mathrm{L}}}{\kappa+\mathrm{i}\left(\Delta_{\mathrm{c}}-\dfrac{g_0^2|c_{\mathrm{s}}|^2}{m_1\omega_1^2-\frac{g_{\mathrm{c}}^2}{m_2\omega_2^2}}\right)+\dfrac{g^2}{\gamma_{\mathrm{a}}+\mathrm{i}\Delta_{\mathrm{a}}}}\right|^2. \tag{7}$$

By rearranging the terms of Eq. (7), and then equating to zero, we obtain a third order polynomial of the steady-state photon number, i.e.,

$$n_{\mathrm{s}}^3+a_0n_{\mathrm{s}}^2+a_1n_{\mathrm{s}}+d=0, \tag{8}$$

where

$$\begin{aligned}
&a_0=\frac{2(\frac{g^2\Delta_{\mathrm{a}}}{\gamma_{\mathrm{a}}^2+\Delta_{\mathrm{a}}^2}-\Delta_{\mathrm{c}})}{\beta},\quad \beta=\frac{g_0^2}{m_1\omega_1^2-\frac{g_{\mathrm{c}}^2}{m_2\omega_2^2}},\quad a_1=\frac{\Gamma}{\beta^2},\\
&\Gamma=\frac{g^2}{\gamma_{\mathrm{a}}^2+\Delta_{\mathrm{a}}^2}(g^2+2\kappa\gamma_{\mathrm{a}}-2\Delta_{\mathrm{c}}\Delta_{\mathrm{a}}),\quad d=\frac{-E_{\mathrm{L}}^2}{\beta^2}.
\end{aligned}$$

Here, $n_{\mathrm{s}}=|c_{\mathrm{s}}|^2$. It is clear that equation (8) has three roots, two are for stable branches and the third one is for the unstable branch of the steady-state photon number. We have found the corresponding regimes of the bistable curve by using the cubic roots equation such that $ax^3+bx^2+cx+d=0$ with inflection and critical points, i.e., $x_{\mathrm{critical}}=\frac{-b\pm\sqrt{b^2-3ac}}{3a}$, $x_{\mathrm{inflection}}=-b/3a$. The inflection point of x is that where the curve changes the concavity. So, we can write

$$n_{\mathrm{s}\pm}=\frac{-a_0\pm\sqrt{a_0^2-3a_1}}{3},\quad n_{\mathrm{s}*}=-a_0/3, \tag{9}$$

where $n_{\mathrm{s}-}$ ($n_{\mathrm{s}+}$) and $n_{\mathrm{s}*}$ are the critical points of lower (upper) stable and unstable branches of the bistable curve. These critical points describe the limit range of bistability window, i.e., $\Delta_{n\mathrm{s}}=n_{\mathrm{s}+}-n_{\mathrm{s}-}$ and have a corresponding window on amplitude of the driving field, i.e., $\Delta(E_{\mathrm{L}})=E_{\mathrm{L}}(n_{\mathrm{s}+})-E_{\mathrm{L}}(n_{\mathrm{s}-})$. Usually, an optomechanical system works in resolved-sideband regime, i.e., $\kappa\ll\omega_m$. Moreover, the strength of the driving field directly affects the resolve-sideband regime; as a result, the photon intensity increases by increasing the strength of the driven field. So we can say that the steady-state photon number exhibits the bistability phenomenon for some specific value of the driving field. The cavity field detuning reaches a certain value with the increase of the driving field, called critical detuning. Hence, at this

value, the threshold bistability in the system can be seen. From Eq. (8), one can find the critical value of the cavity field detuning like this

$$\Delta_{\rm c} = \sqrt{3}\kappa. \tag{10}$$

Equation (10) represents the condition for the critical value of the cavity field detuning in the absence of atom-field coupling as well as Coulomb coupling. However, this condition is modified by considering these couplings. Therefore, we have

$$\Delta_{\rm c} = \frac{g^2\Delta_{\rm a}}{\gamma_{\rm a}^2+\Delta_{\rm a}^2} + \sqrt{3\left(\kappa^2+\left(\frac{g^2}{\gamma_{\rm a}^2+\Delta_{\rm a}^2}\right)(g^2+2\kappa\gamma_{\rm a})\right)}. \tag{11}$$

To analyze the optical bistability and FWM in NEOMS, we select the parametric values from the available experiments[26,79,80] as well as from theoretical work closer to experiment.[72,73] We have considered that the nanomechanical resonator $\rm NMR_1$ ($\rm NMR_2$) oscillates with frequency $\omega_1(\omega_2) = 2\pi \times 947$ kHz. Other parameters are: field frequency $\omega_{\rm c} = 2\pi \times 15.3 \times 10^{14}$ Hz, field decay rate $\kappa/2\pi = 215$ kHz, quality factor $Q = 6700$, decay rate of $\rm NMR_1$ ($\rm NMR_2$) $\gamma_1(\gamma_2) = \frac{\omega_1(\omega_2)}{Q}$, mass of $\rm NMR_1$ ($\rm NMR_2$) $m_1 = m_2 = 145$ ng, and the detuning frequency $\delta = \omega_1(\omega_2)$. Typically $N = 10^5$ ^{87}Rb atoms are coupled to the laser field, and the wavelength of the driving field $\lambda_{\rm L} = 1064$ nm, laser power $\wp_1 = 12$ mW, and cavity length $L = 25$ mm. The strength of the pump field $E_{\rm L}/2\pi = 20$ MHz, atom-field frequency $g = g_{\rm a}\sqrt{N}/2\pi = 40$ kHz, mirror-field frequency $g_0/2\pi = 8$ kHz, Coulomb frequency $g_{\rm c}/2\pi = 100$ kHz, atom-field detuning $\Delta_{\rm a}/2\pi = 30$ kHz with decay rate $\gamma_{\rm a}/2\pi = 0.1$ kHz, and cavity-field detuning $\Delta_{\rm c} = 3\kappa$.

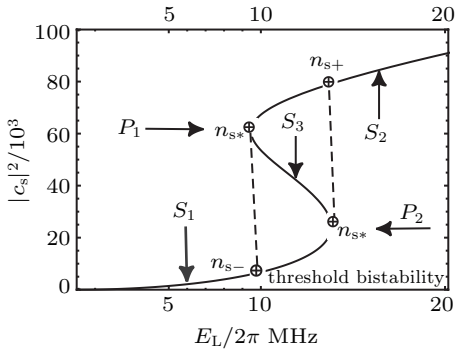


Fig. 2. The steady-state photon number $|c_{\rm s}|^2$ is demonstrated against the driving field of amplitude $E_{\rm L}$. The parameter values in this particular case are taken as $g = g_{\rm a}\sqrt{N}/2\pi = 10$ kHz, $g_0/2\pi = 3.5$ kHz, $g_{\rm c}/2\pi = 100$ kHz, $\Delta_{\rm c} = 3.5\kappa$, $\gamma_{1,2} = \omega_{1,2}/Q$, $\Delta_{\rm a}/2\pi = 20$ kHz, and $\gamma_{\rm a}/2\pi = 0.1$ kHz.

The steady-state solution of Eq. (7) is sketched in Fig. 2 (bifurcation diagram) by taking cavity field detuning $\Delta_{\rm c} = 3.5\kappa$ against the variation of input driving field. The critical points $n_{\rm s-}$ and $n_{\rm s+}$ correspond to lower and upper stable branches and the inflection point $n_{\rm s*}$ corresponds to the unstable branch of the bistable curve. If we start scanning with a low driving field $E_{\rm L}$, and gradually increase the driving field frequency, the intra-cavity intensity initially follows the lower stable branch S_1 of the cubic, which extends from the origin to the first critical point $P_1(n_{\rm s*})$. When the amplitude of the driving field reaches to $2\pi \times 14$ MHz, the lower stable branch jumps to the upper stable branch S_3, which extends from the critical point P_2 $(n_{\rm s*})$ to infinity. Keep continuing to increase the value of $E_{\rm L}$, the lower stable branch will continue to follow the upper stable branch. The center branch denoted by S_2 is unstable and extends between the two inflection points $P_1(n_{\rm s*})$ and $P_2(n_{\rm s*})$. Note that the unstable branch S_2 should be negative and cannot be experimentally observed. Further, it is noteworthy that the condition is compatible with the fact that the branches with negative slope are always unstable. On the other hand, if $E_{\rm L}$ decreases from $2\pi \times 20$ MHz, the intra-cavity photon number will be found decreasing by following the upper branch at first; however, whenever it reaches the second critical point $P_2(n_{\rm s*})$, it will jump down to the lower stable branch and continue to decrease further along that branch.

Next, we provide a detailed analysis of electro-optomechanical switch based on tunable bistability that depends on system parameters. Figure 3(a) represents the S-shaped (bifurcation) curve of the steady-state intra-cavity photon number $|c_{\rm s}|^2$ and shows its variation against the amplitude $E_{\rm L}$ for different atom-field coupling frequencies. Keep in mind that the curves overlap for different values of atom-field coupling. For $g/2\pi = 20$ kHz (black solid curve), the bistable curve lies at its upper stable branch and exhibits maximum photon number of the cavity field. But, the higher stable branch jumps to its lower stable branch once we increase the atom field coupling to $2\pi \times 30$ kHz (blue dotted curve); the width of the curve also decreases and critical points of the stable branch come closer, which exhibits low photon number. Further, by increasing the strength of the atom field coupling, the bistable branch jumps step by step to its lower branch for $g/2\pi = 40$ kHz (red dashed curve) and $g/2\pi = 50$ kHz (green thick dashed curve). The width of the bistable curve decreases and becomes narrow and narrow for higher values of atom-field coupling. On the other hand, if we consider the minimum values of atom-field coupling, the lower stable branch will follow the upper stable branch. Thus figure 3(a) elucidates that the atom-field coupling has greater influence on bistability and allows us to design an optical switch that can be controlled by atom-field coupling.

Similarly, we can also think an optical switch that can be tuned by Coulomb coupling. For this purpose, we plot the bistable curve of the intra-cavity photon number $|c_{\rm s}|^2$ versus driving field for different frequencies of $g_{\rm c}$ as given in Fig. 3(b). We have tuned the system for several values of $g_{\rm c}$ through V_1 and $-V_2$. When the potential difference across each mechanical resonator is low, the Coulomb coupling be-

tween resonators is not strong enough, i.e., $g_c/2\pi = 100$ kHz (black solid curve), we have maximum photon number and the system lies in the upper stable branch. When the voltage difference across each resonator increases, the charge also increases on each resonator. It enhances the Coulomb interaction as well as the radiation pressure force between the resonators. The non-linearity in the system increases and the intra-cavity photon number $|c_s|^2$ is suppressed inside the cavity. We observe this behavior in Fig. 3(b) for $g_c/2\pi = 150$ kHz (blue dotted curve), $g_c/2\pi = 200$ kHz (red dashed curve), and $g_c/2\pi = 250$ kHz (green solid curve). This analysis reveals that Coulomb coupling has a remarkable effect on bistable behavior of the steady-state photon number along with the driving field.

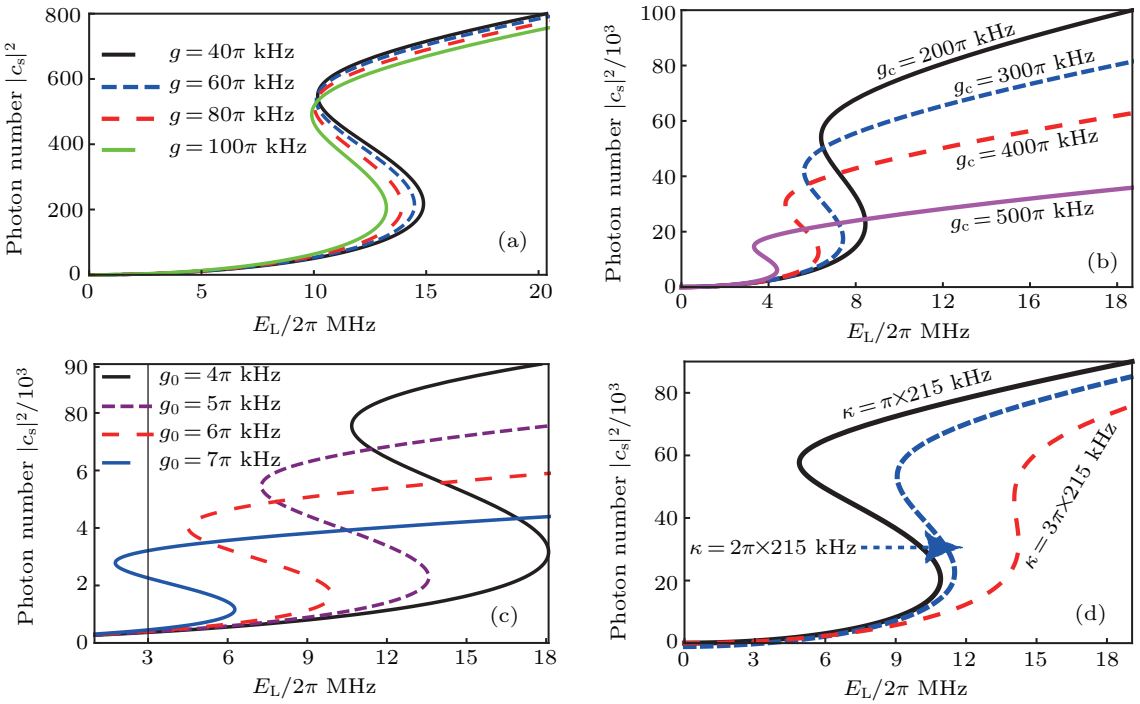


Fig. 3. (a) The variation in the intra-cavity photon intensity $|c_s|^2$ is shown against the amplitude of the driving field E_L for different cases of g, g_c, g_0, and κ, respectively. The black solid, blue dotted, red dashed, and green longer dashed curves represent the bistable information for four different values of (a) $g/2\pi = (20, 30, 40, 50)$ kHz, (b) $g_c/2\pi = (100, 150, 200, 250)$ kHz, and (c) $g_0/2\pi = (2, 2.5, 3, 3.5)$ kHz, while in panel (d), black solid, blue dotted, and red dashed curves exhibit the bistable behavior for three different values of $\kappa/2\pi = (0.5, 1.0, 1.5)215$ kHz. We take $g_0 = 2\pi \times 4$ kHz in panels (a,b,d), $g/2\pi = 20$ kHz in panels (b,c,d), while $\gamma_{1,2} = \omega_{1,2}/Q$, $\Delta_a/2\pi = 200$ kHz, and $\gamma_a/2\pi = 0.1$ kHz remain the same in each panel.

In Fig. 3(c), we show the bistable behavior of the photon intensity $|c_s|^2$ versus the variation of the driving field for several coupling frequencies of g_0. In the present scenario, the radiation pressure increases corresponding to the input field, as a result, strengthening the mirror-field coupling frequency. The interaction of NMR_1 with cavity field raises the radiation pressure force, which causes the scattering of photon intensity in the cavity. At lower value of optomechanical coupling, i.e., $g_0/2\pi = 2.0$ kHz (black solid curve), the bistable curve follows the upper stable branch. When the frequency of the optomechanical coupling gradually increases, the upper stable path follows the lower stable path for $g_0/2\pi = 2.5$ kHz (blue dashed curve). The width of the bistable curve also decreases at the same time by increasing the frequency of g_0. Further, strengthening the frequency of the optomechanical coupling, the second lower stable branch follows the third lower stable branch and vice versa. So far, there is a continuous variation in the bistable curve as well as in photon number with the variation of g_0. The variation in photon number is also called flip-flop phenomenon. It means that the control of the intra-cavity photon intensity is a function of optomechanical coupling. Moreover, this control parameter provides a possibility of a realizable controllable optical switch.

Now, we examine the effect of the cavity decay rate κ on optical bistability. Therefore, we display the bistable behavior of the intra-cavity photon number against the driving field for various decay rates of the cavity field, as sketched in Fig. 3(d). Here, we have found that by increasing the decay rate, as a result, the width of the bistability window decreases. The black curve represents smaller cavity field decay κ, and maximum steady-state photon number is seen for $\kappa/2\pi = 0.5 \times 215$ kHz. When decay rate increases (the loss in cavity field increases), the photon number decreases, therefore, the stable branch goes to lower stable branch for $\kappa/2\pi = 215$ kHz (blue dashed curve). At this time, the photon number is low and branch points come closer. Further, by strengthening the cavity decay rate, the cavity detuning field becomes larger and generates bifurcation phenomenon in the

cavity. This suppresses the steady-state photon number, as a result, we have low photon number and shift the upper stable branch to lower stable branch. Hence, from the discussion of Fig. 3(d), it is concluded that increasing the decay rate of the cavity field, the maximum photon number is suppressed, and thus bistable curve keeps continuing jumping from upper stable branch to a lower stable in successive steps.

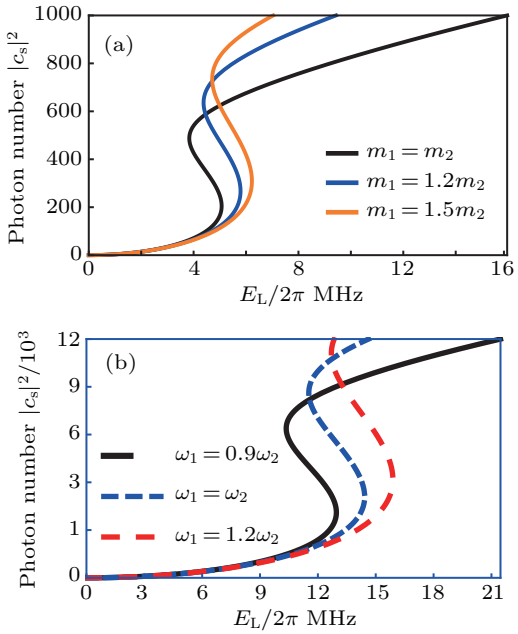


Fig. 4. The bistable behavior of the intra-cavity photon number $|c_s|^2$ is shown versus the amplitude of the driving field E_L for several masses of NMR$_1$ (NMR$_2$). (a) The black, blue, orange curves represent the bistable information for $m_1 = m_2$, $m_1 = 1.2m_2$, and $m_1 = 1.5m_2$, respectively. (b) The several colors represent the variation in photon intensity for various frequencies, i.e., $\omega_1 = 0.9\omega_2$, $1.0\omega_2$, and $1.2\omega_2$. Other parameters are counted as $\omega_{1,2}/2\pi = 947$ kHz, $\kappa/2\pi = 215$ kHz, $g_c/2\pi = 100$ kHz, $g/2\pi = 10$ kHz, $\Delta_a/2\pi = 20$ kHz, and $\Delta_c = 3\kappa$.

Next, we explain the optical bistability of NEOMS by considering different oscillators and show whether the photon bistable behavior increases or decreases. In Figs. 4(a) and 4(b), we display the bistable behavior of the steady-state photon number for different oscillators against the driving field E_L. Figure 4(a) indicates that, if the mass of NMR$_1$ is gradually increased corresponding to NMR$_2$, the bistable curve of the NEOMS will move from lower stable branch to upper stable branch. But in contrast, the masses of the resonators are decreased, and the bistable behavior of the NEOMS will exhibit reverse behavior. Further, in Fig. 4(b), we sketch the bistable behavior of the NEOMS against the amplitude of the driving field E_L for different frequencies of NMR$_1$ corresponding to NMR$_2$. We see at lower frequency of NMR$_1$, i.e., $\omega_1 = 0.9\omega_2$, the bistable curve lies in its lower stable regime as labeled by black solid curve. However, operating higher frequencies of NMR$_1$ corresponding to NMR$_2$, i.e., $\omega_1 = 1.0\omega_2$, $1.2\omega_2$, the bistable behavior increases and the thickness of the curve becomes broadened. This means that considering different mechanical resonators corresponding to the higher frequencies, the bistable behavior of the NEOMS increases and lies at its upper branch. Moreover, the same bistable behavior for steady-state position can be observed by considering different masses and frequencies of NMR$_j$.

In Figs. 5(a)–5(d), the bistable behavior of the steady-state position q_{1s} (q_{2s}) of the mechanical mode NMR$_1$ (NMR$_2$), corresponding to the steady-state component in Eq. (4), is plotted as a function of the driving field. We observe that the bistable behavior of the first mechanical mode NMR$_1$ occurs at a certain regime for different values of optomechanical coupling and atom-field coupling, respectively. Moreover, figures 5(a) and 5(b) show the bistable behavior of the mechanical modes of the hybrid NEOMS and describe their collective influence on atom-field coupling as well as on optomechanical coupling. In Fig. 5(a), there is a slight change in the bistable curve from $g/2\pi = 10$ kHz (black solid curve) to $g/2\pi = 20$ kHz (blue dashed curve). Moreover, when the atom-field coupling g is smaller than $\omega_1(\Delta_a)$, it barely changes the bistable curve of q_{1s}. However, multistable behavior can be observed, when the atom-field coupling and the mechanical modes become very strong or ultra-strong.

Similarly, figure 5(b) represents the bistable behavior of the steady-state position of NMR$_1$. We know that optomechanical coupling is more sensitive as compared to atom-field coupling. If we slightly change the coupling frequency of NMR$_1$, the bistable curve shows a prominent change in the steady-state position q_{1s} of NMR$_1$. The solid black, blue dotted, red dashed, and purple curves show variation in the mechanical steady-state position q_{1s} in a descending order by selecting different coupling frequencies $g_0/2\pi = (2, 2.5, 3, 3.5)$ kHz. Moreover, dealing with higher optomechanical coupling frequencies, the nonlinearity increases in the system, as a result, bistable curve jumps from upper stable branch to the lower branch. In this way, an optical switch can be realized by using the pump field as input and optomechanical coupling as the control.

Next, we investigate the bistable behavior of the mechanical steady-state position q_{2s} by operating different frequencies of the cavity field detuning and Coulomb coupling, respectively. Therefore, in Figs. 5(c) and 5(d), we illustrate the bistable behavior of the mechanical steady-state position q_{2s} as a function of pump field for several values of Δ_c and g_c. The stable and unstable points are changed by changing the cavity field detuning and Coulomb coupling. It is clear that from Figs. 5(c) and 5(d), the S-shaped shows reverse behavior of Figs. 5(a) and 5(b). We see that the upper branch of the bistable curve jumps to next upper stable branch for higher values of cavity field detuning and Coulomb coupling. In this case, the bistable behavior of the steady-state position q_{2s} increases and follows higher stable branches by operat-

ing $\Delta_c = (2.0, 2.5, 3.0)\kappa$ and $g_c/2\pi = (100, 120, 140)$ kHz, respectively. A similar transition occurs from the upper stable branch to the lower stable branch with the decreasing strength of the driving field. These observations realize the fact that the origin of the bistable behavior is the inherent non-linearities of Δ_c, E_L, and g_c, respectively. This shows that we can develop an optical switch that can be controlled by cavity field detuning and amplitude of the driving field.

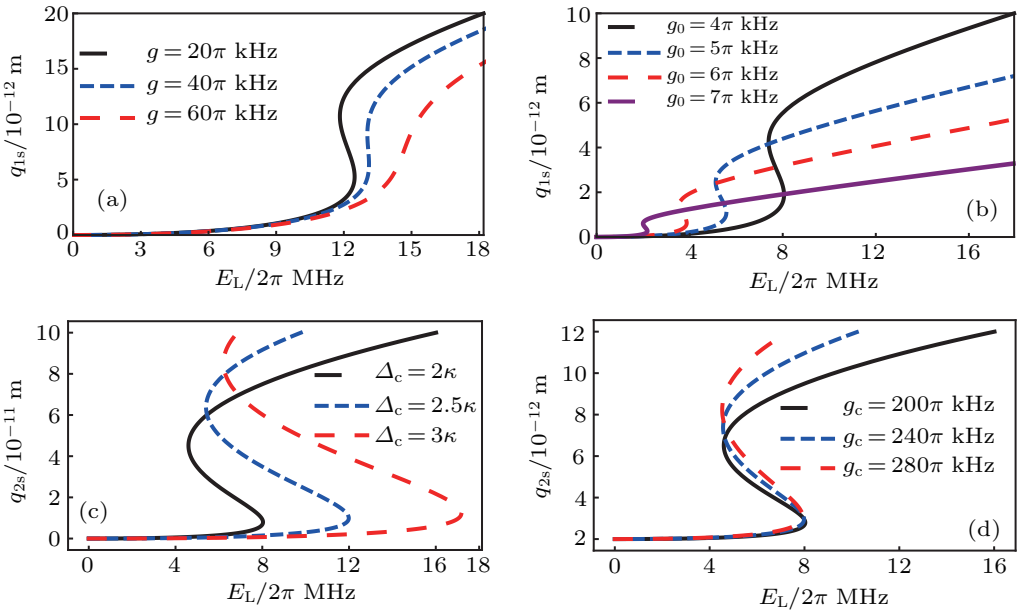


Fig. 5. The bistable behavior of the steady-state position q_{1s} is plotted as a function of driving field for different cases: (a) $g/2\pi = 10$ kHz, 20 kHz, and 30 kHz; (b) $g_0/2\pi = (2, 2.5, 3.0, 3.5)$ kHz. The variation in the steady-state position q_{2s} is sketched as a function of driving field for several values of cavity field detuning, i.e., Δ_c, and Coulomb coupling g_c in panels (c) and (d), respectively. Other parameters are considered as $\Delta_a/2\pi = 10$ kHz, $\gamma_{1,2} = \omega_{1,2}/Q$, $\gamma_a/2\pi = 0.1$ kHz, $\Delta_c = 3\kappa$, and $g_c/2\pi = 100$ kHz.

Here, we are going to introduce other possibilities of an optical switch in electro-optomechanical system with the necessity of using different scanned parameters. The first possibility is shown in Fig. 6(a) by tuning optomechanical coupling for its different frequencies. We see that the bistability curve bends low towards right at $g_0/2\pi = 10$ kHz (black solid curve) and lies at its near stable regime and has low photon number. But for $g_0/2\pi = 12$ kHz, the curve becomes more bended and pushed the system to its lower stable branch, see blue solid line in Fig. 6(a). Further, increasing the values of optomechanical coupling to $g_0/2\pi$ =(14 kHz, 16 kHz), see the red and yellow lines, the bistable curve further moves to lower and lower stable regime. Hence, in this way, we can enable or disable an optical switch by using different values of g_0.

The other possibility of an optical switch is by tuning the Coulomb coupling through different potential difference on NMR_1 and NMR_2. It is clear that from Fig. 6(b), the stability of the NEOMS moves from higher stable point to lower stable point at higher value of g_c. The stability curve becomes more and more bended as we increase the values of g_c and produces a great change in the photon number. This shows that we can develop an optical switch which is controlled by the potential difference across each resonator. Similarly, figure 6(c) displays the bistability of the intra-cavity photon intensity versus normalized atom-field detuning Δ_a/ω_l. The stability curve is quite straight and there is no significant difference between the width of the peak versus Δ_a/ω_l for different values of atom-field coupling. The system shows a slight change in stable points of the bistable curve by operating different values of atom-field coupling. The bistability is maximum at $g/2\pi = 2$ kHz (black curve), and $g/2\pi = 3$ kHz (red curve) and the photon number has maximum intensity. Increasing the values of atom-field coupling, the stability curve shows small change from stable to the unstable point for $g/2\pi = 4$ kHz, 5 kHz (blue and yellow curves).

In Fig. 6(d), the bistable behavior of the steady state photon number $|c_s|^2$ is plotted against the normalized cavity field detuning Δ_c/κ for four different values $\omega_l = 1.0\omega_2$, $1.1\omega_2$, $1.2\omega_2$, and $1.3\omega_2$. In this case, the bistability curve has a reverse character of Fig. 6(c). The width of the bistability curve and photon number increases with the increase of the frequencies of NMR_1 corresponding to NMR_2. The curve becomes much straighter for $\omega_l = 1.3\omega_2$ which exhibits maximum photon number. We observe that the obtained threshold bistability in an optomechanical system consists of double end moving coupled-charged resonators, the frequency of each resonator as to control.

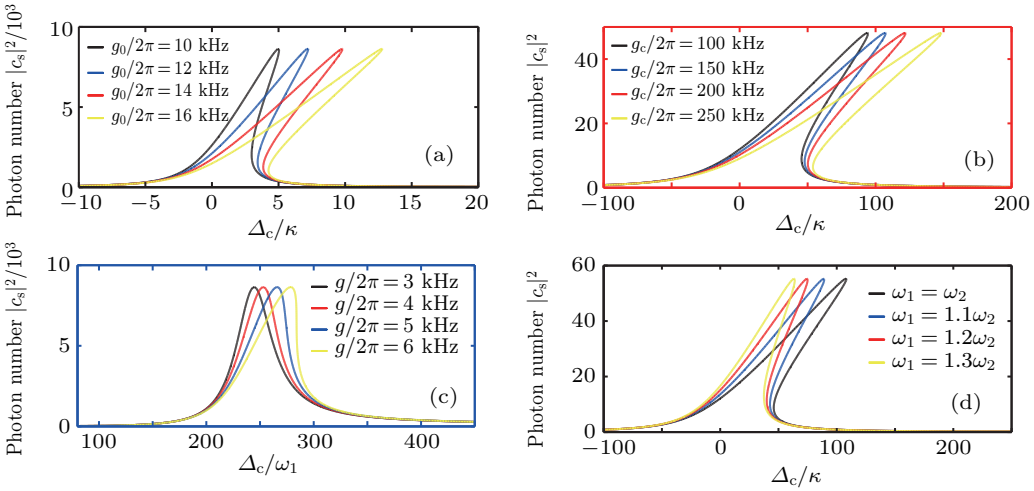


Fig. 6. A sketch of the steady-state photon number $|c_s|^2$ against the normalized cavity field detuning Δ_c/κ for the cases (a) $g_0/2\pi = (10, 12, 14, 16)$ kHz; (b) $g_c/2\pi = (100, 150, 200, 250)$ kHz. (c) The steady state mean intra-cavity photon numbers $|c_s|^2$ against the normalized atomic detuning Δ_a/ω_1 for different values of atom field coupling $g = g_a\sqrt{N}$. (d) The steady state mean photon number $|c_s|^2$ against the dimensionless detuning Δ_c/κ for four different frequencies of NMR_1. The remaining parameters are the same as used in Fig. 9.

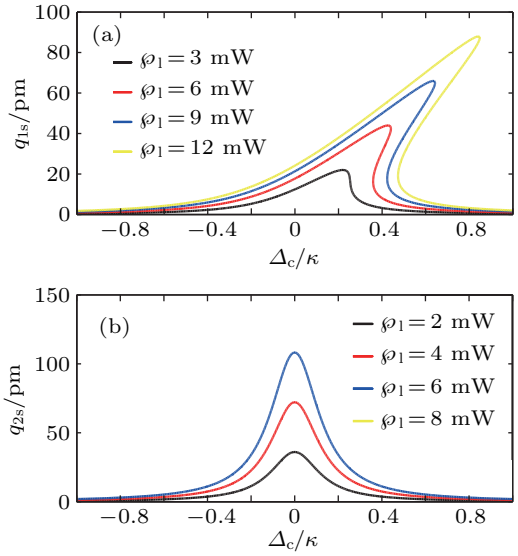


Fig. 7. The steady-state positions q_{1s} and q_{2s} of the mechanical modes NMR_1 and NMR_2 are illustrated against the cavity field detuning Δ_c/κ for four different input powers $\wp_1$. Other parameters are $\Delta_a/2\pi = 200$ kHz, $\gamma_{1,2} = \omega_{1,2}/Q$, $\gamma_a/2\pi = 0.1$ kHz, $g_0 = 8\pi$ kHz, $g/2\pi = 20$ kHz, and $g_c/2\pi = 100$ kHz.

To demonstrate the effect of laser power $\wp_1$ on bistable behavior of the steady-state positions q_{1s} and q_{2s}, therefore, in Figs. 7(a) and 7(b), we plot q_{1s} and q_{2s} versus normalized cavity field detuning Δ_c/κ for different values of pump power $\wp_1$. The behavior of the curve in Fig. 7(a) is near Lorentzian at $\wp_1 = 3$ mW, while in Fig. 7(b), the curve exhibits complete Lorentzian shape at $\wp_1 = 2$ mW. This means that the bistable curve of the steady-positions q_{1s} and q_{2s} lies at its lower stable branch and we have a symmetrical Lorentzian curve centered at $\Delta_c = 0$. The Lorentzian curve in Fig. 7(b) remains unchanged by increasing the input power $\wp_1$ and only gains the height, but in Fig. 7(a), the curve changes direction and shifts toward right as we increase the value of $\wp_1$. It becomes more and more symmetric as we further strengthen the input power. The peak gets height and becomes wider at higher values of laser power; however, no changes are observed in its direction. Moreover, dealing with different higher laser powers, the bistable behavior of the steady-state position q_{2s} reaches a threshold bistability at critical power. However, by selecting weak laser power, the peak height becomes shorter and shorter. In this case, the system will shift towards lower stable branch, as a result, the steady-state position q_{1s} (q_{2s}) exhibits lower bistable behavior. From the above discussions, we can say that the occurred bistability in the nano-electro-optomechanical system enables a controlled bistable switching of the photon intensity and mechanical steady-state positions by appropriately adjusting the input power and cavity field detuning frequency.

4. Four-wave mixing intensity

Here, we investigate the FWM intensity in the hybrid nano-electro-optomechanical system. First, we discuss the analytic approach of the FWM intensity by calling input-output theory[82]

$$\begin{aligned}\hat{c}_{\rm out} &= \sqrt{2\kappa}\hat{c} - \hat{c}_{\rm in},\\ \hat{c}_{\rm out} &= \sqrt{2\kappa}\Bigg[\left(\hat{c}_{\rm s} - \frac{E_{\rm L}}{\sqrt{2\kappa}}\right)e^{-i\omega_{\rm L}t}\\ &\quad + \left(\hat{c}_{-} - \frac{\varepsilon_{\rm p}}{\sqrt{2\kappa}}\right)e^{-i(\omega_{\rm L}+\delta)t} + \hat{c}_{+}e^{-i(\omega_{\rm L}-\delta)t}\Bigg]. \quad (12)\end{aligned}$$

Here, $\delta = \omega_{\rm p} - \omega_{\rm L}$. In Eq. (12), the first term corresponds to the output driving field with amplitude $E_{\rm L}$ and frequency $\omega_{\rm L}$. The second and third terms appear due to probe field having frequencies $\omega_{\rm p}$ and $2\omega_{\rm L} - \omega_{\rm p}$, respectively. Moreover, the frequency $2\omega_{\rm L} - \omega_{\rm p}$ in the third term of the output field corresponds to the Stoke field. In addition, the second term is related to electro-mechanical induced transparency (EMIT),

whereas the third term generates the nonlinear effect in the system which is called four-wave mixing. In four-wave mixing process, the two photons of the driving field interact with a single photon of the probe field each with frequencies $\omega_{\rm L}$ and $\omega_{\rm p}$, generating a new photon of frequency $2\omega_{\rm L}-\omega_{\rm p}$. In this process, the two input frequencies are selected in such a way that $\omega_{\rm L}-\omega_{\rm p}$ is near a transition of a dielectric medium, such as coherent Raman scattering. The four-wave mixing intensity enhances the non-linear effect in the system, especially in nano-electro-optomechanical system which behaves as a three-mode coupled system. The coherent driving field frequency as well as the probe field frequency remains invariant during reflection, transmission, and refraction in a nonlinear medium via elastic scattering. Hence, the energy and momentum are both conserved during the interaction of field frequencies. In another perspective, the energy transfer is a coherent process and the four-wave must retain a constant phase, relative to the others, in order to avoid any destructive interference.[82] Using the steady state operator in Eq. (5) and after some simplification, we obtain the FWM term like this

$$c_{+}=\frac{{\rm i}\varepsilon_{\rm p}\eta\zeta}{(X+Y-{\rm i}\eta)(X'+Y'-{\rm i}\eta')-\eta^2}, \tag{13}$$

where

$$\begin{aligned}
&\eta=g_0^2|c_{\rm s}|^2m_2(\omega_2^2-\delta^2+{\rm i}\delta\gamma_2),\\
&\zeta=m_1m_2(\omega_1^2-\delta^2+{\rm i}\delta\gamma_1)(\omega_2^2-\delta^2+{\rm i}\delta\gamma_2)-g_{\rm c}^2,\\
&X=\kappa+{\rm i}(\Delta+\delta)\zeta,\quad Y=\frac{g_{ac}^2N\zeta}{\gamma_{\rm a}+{\rm i}(\Delta_{\rm a}+\delta)},\\
&X'=\kappa-{\rm i}(\Delta-\delta)\zeta',\quad Y'=\frac{g_{ac}^2N\zeta'}{\gamma_{\rm a}-{\rm i}(\Delta_{\rm a}-\delta)},\\
&\eta'=g_0^2|c_{\rm s}|^2m_2(\omega_2^2-\delta^2-{\rm i}\delta\gamma_2),\\
&\zeta'=m_1m_2(\omega_1^2-\delta^2-{\rm i}\delta\gamma_1)(\omega_2^2-\delta^2-{\rm i}\delta\gamma_2)-g_{\rm c}^2.
\end{aligned}$$

Here, $\zeta'(\delta)=\zeta(-\delta)$, $\eta'(\delta)=\eta(-\delta)$, and $X'(\delta)=X(-\delta)$. The normalized FWM intensity in term of probe field can be written as

$${\rm FWM}=\left|-\frac{\sqrt{2\kappa}c_{+}}{\varepsilon_{\rm p}}\right|^2. \tag{14}$$

In Fig. 8(a), we display the FWM intensity against the normalized probe field detuning $\delta/\omega_{\rm l}$ for several values of optomechanical coupling g_0, while keeping the absence of the atom-field coupling g as well as the electrostatic Coulomb coupling $g_{\rm c}$. When optomechanical coupling g_0 is insufficiently strong, the FWM intensity is far away from resonant regime. The curve has a narrow width at $g_0/2\pi=5$ kHz (black curve) and consists of symmetric single peak centered at $\delta/\omega_{\rm l}=1$. This represents the single photon resonant process. Such behavior was previously studied in a two-mode optomechanical system,[64] where different powers were operated for photon resonance process. Here, we discuss the four-wave mixing process in a tripartite system operated by a single mode cavity field along with different optomechanical couplings. Figure 8(a) indicates that increasing the value of optomechanical coupling to $g_0/2\pi=6$ kHz (blue curve), the FWM intensity moves toward the near-resonant regime and the width of the curve becomes broadened. Further, increasing the optomechanical coupling frequency to its critical values, i.e., $g_0/2\pi=(7,8)$ kHz, the FWM intensity reaches the resonant regime. As a result, the red and orange curves are apparently split into two asymmetric peaks centered at $\delta/\omega_{\rm l}=0.89,0.8$ on the left and $1.1,1.15$ on the right side with single dip centered at $\delta/\omega_{\rm l}=1$. Thus we have observed two-photon resonant process. Also, the magnitudes of the sideband and interior peaks are increased with the increase of g_0. In addition, the FWM is not suppressed at resonance regime, i.e., $\delta=\omega_{\rm l}$, it is because of constructive interferences of the reflected and transmitted fields to the coupling field of NMR$_1$. Therefore, the FWM intensity has apparent normal mode splitting in Fig. 8(a). In this case, not only the probe field but also the driving field is stored inside the cavity. It is kept in mind that when the optomechanical coupling is switched off ($g_0=0$), there will be no FWM intensity that can be seen amongst reflected, transmitted, and coupling fields. Therefore, optomechanical coupling plays a vital role in generating the FWM intensity.

Figure 8(b) displays the FWM intensity against the normalized probe field detuning for several values of optomechanical coupling g_0 in the presence of Coulomb coupling $g_{\rm c}$, but the atom-field coupling is kept absent ($g=0$). Here, we examine the impact of Coulomb coupling on FWM intensity with the variation of g_0. In the present scenario, figure 8(b) has larger peak separation as compared to Fig. 8(a) for the same value of optomechanical coupling g_0, however, no additional peak appears. This shows the verification of Eq. (8) that Coulomb coupling is independent of the cavity field and only depends on optomechanical coupling. Therefore, if we switch off g_0, Coulomb coupling will automatically switch off ($g_{\rm c}=0$). Here, we see that in Fig. 8(b), the black curve appears double peaks instead of single peak as appeared in Fig. 8(a) for $g_0/2\pi=5$ kHz. The results of Fig. 8(b) reflect the previous results of FWM in a composite photonic molecule optomechanics,[65] which was previously discussed at different detunings, i.e., red detuning and blue detuning. Moreover, in Ref. [65], it has been observed that the FWM intensity decreases with the increase of pump power at red detuning while increases with the increase of pump power at blue detuning. Since our system works at red sideband regime (red detuning), therefore, we explain the FWM intensity with a different approach and hence, photon intensity increases rather than decreases like Ref. [65]. Figure 8(b) indicates that the combined coupling frequency of g_0 and $g_{\rm c}$ has a greater radiation pres-

sure than from the optomechanical coupling frequency alone. In other words, the Coulomb coupling is responsible to enhance the strength of optomechanical coupling g_0. The result presented in Fig. 8(b) shows that the full width at half maximum (FWHM) increases and the amplitude of the FWM also increases by turning the NMR_1 coupling from weak coupling ($g_0/2\pi = 5$ kHz) to strong coupling ($g_0/2\pi = 8$ kHz). Moreover, when the value of the optomechanical coupling g_0 lies in a certain range, bistable behavior of intra-cavity photon number can exist, where intra-cavity photon number n_s determined by Eq. (8) has three possible real values, respectively, the largest and smallest are stable, and the middle one is unstable as discussed in the previous section. It is to be noted that the FWM intensity decreases with the increase of the probe field detuning and becomes zero at $\delta = \omega_1$. At this frequency, the photons are completely suppressed inside the cavity and destructive interference has occurred. Therefore, the FWM intensity process is completely suppressed at resonance regime and only the probe field is stored inside the system.

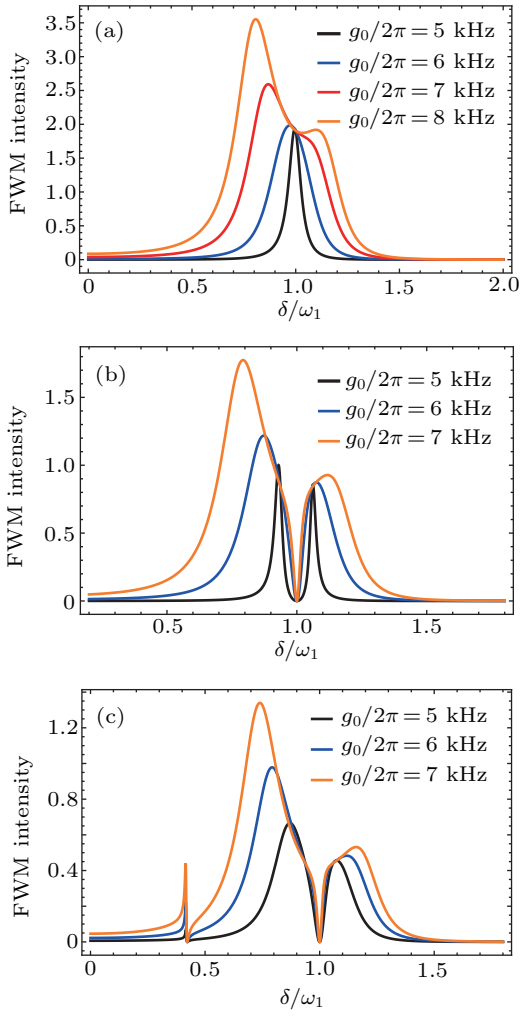


Fig. 8. The display of the FWM intensity versus the dimensionless frequency δ/ω_1 for different values of optomechanical coupling g_0 for the cases: (a) both atom field coupling and Coulomb coupling are zero, i.e., $g = 0$ and $g_c = 0$; (b) $g = 0$ and $g_c \neq 0$; (c) $g \neq 0$ and $g_c \neq 0$. Other parameters are $\gamma_1 = \omega_1/Q$, $\gamma_a/2\pi = 0.1$ kHz, $g_c/2\pi = 100$ kHz, $\kappa/2\pi = 215$ kHz, $g/2\pi = 10$ kHz, and $E_L = 2\pi \times 20$ MHz.

At last, we examine the behavior of FWM intensity for different optomechanical couplings by introducing the atom-field coupling. We plot the FWM intensity in Fig. 8(c), defined in Eq. (14), against the normalized probe field detuning for several values of optomechanical coupling. The infix of Fig. 8(c) shows the origin of this triple-peaked structure which is appropriated to a three-photon resonance process. It is clear that once we introduce the atom–field coupling, an additional peak appears. The peaks become broadened as we increase the optomechanical coupling. Moreover, in Fig. 8(c), the amplitudes and separation of the peaks are increased to higher values for larger values of g_0. We note the shifted detuning centered at $\delta/\omega_1 = 0.9$, 0.8, 0.75 on the left side and 1.12, 1.17, 1.22 on the right. One can see that in Fig. 8(c), the amplitude of atom-field frequency has only one peak centered at $\delta/\omega_1 = 0.4$.

From the above discussion, we conclude that in the presence of atom-field and Coulomb couplings, NEOMS faces with a high degree of non-linearity and most of the intra-cavity photons are stimulated; as a result, the FWM intensity decreases which is clearly indicated in Figs. 8(b) and 8(c). The FWM intensity can be enhanced by increasing the optomechanical coupling or increasing the input driven power or decreasing the probe field detuning. In other words, the FWM process of the hybrid NEOMS can be controlled by adjusting the optomechanical coupling corresponds to the input driving field and probe field detuning.

5. Conclusion

We present an experimentally realizable scheme to realize an electro-optomechanical switch based on optical bistability and FWM intensity in a hybrid nano-electro-optomechanical system in the presence of two-level atoms trapped inside a Fabry–Pérot cavity. We report the existence of optical bistability in steady-state photon number as a function of mirror field coupling, atom-field coupling, and Coulomb coupling along with different resonators. In the studied system, the parameters allow a considerable threshold value of the cavity detuning and power which can be useful for the tremendous applications in developing optical switches at manageable intensities. Moreover, we have explained that the FWM intensity process is the function of optomechanical coupling and no FWM can be observed when the optomechanical coupling is switched off. Further, we have observed that the FWM intensity has one peak at low resonant regime when both electrostatic Coulomb coupling and atom-field coupling are absent. In the presence of atom-field coupling and Coulomb coupling, the FWM intensity exhibits three peaks due to the additional frequency in the system. Hopefully, our reported results can be applied in designing all-optical switch, storage of optical pulse signals, optical transistors, and the memory devices.

Acknowledgment

The author greatly acknowledge support from the staff of the Department of Physics, Quaid-i-Azam University (QAU) Islamabad. The author would like to thank the anonymous referees for their insightful comments which have greatly improved this paper.

References

[1] Rugar D, Budakian R, Mamin H J and Chui B W 2004 *Nature* **430** 329
[2] Schwab K C and Roukes M L 2005 *Phys. Today* **58** 36
[3] Rocheleau T, Ndukum T, Macklin C, Hertzberg J B, Clerk A and Schwab K C 2010 *Nature* **463** 72
[4] Arcizet O, Jacques V, Siria A, Poncharal P, Vincent P and Seidelin S 2011 *Nat. Phys.* **7** 879
[5] Kippenberg T J and Vahala K J 2008 *Science* **321** 1172
[6] Aspelmeyer M, Groblacher S, Hammerer K and Kiesel N 2010 *J. Opt. Soc. Am. B* **27** A189
[7] Aspelmeyer M, Meystre P and Schwab K 2012 *Phys. Today* **65** 29
[8] Brennecke F, Ritter S, Donner T and Esslinger T 2008 *Science* **322** 235
[9] Treutlein P, Hunger D, Camerer S, Hänsch T W and Reichel J 2007 *Phys. Rev. Lett.* **99** 140403
[10] Xiang Z L, Ashhab S, You J Q and Nori F 2013 *Rev. Mod. Phys.* **85** 623
[11] Jöckel A, Faber A, Kampschulte T, Korppi M, Rakher M T and Treutlein P 2015 *Nature Nanotechnology* **10** 55
[12] Bariani F, Singh S, Buchmann L F, Vengalattore M and Meystre P 2014 *Phys. Rev. A* **90** 033838
[13] Saffman M, Walker T G and Mflmer K 2010 *Rev. Mod. Phys.* **82** 2313
[14] Jaksch D, Cirac J I, Zoller P, Rolston S L, Côté R and Lukin M D 2000 *Phys. Rev. Lett.* **85** 2208
[15] Weimer H, Müller M, Lesanovsky I, Zoller P and Buchler H P 2010 *Nat. Phys.* **6** 382
[16] Dobrindt J M, Wilson-Rae I and Kippenberg T J 2008 *Phys. Rev. Lett.* **101** 263602
[17] Rokhsari H, Kippenberg T J, Carmon T and Vahala K J 2005 *Opt. Exp.* **13** 5293
[18] Ian H, Gong Z R, Liu Y X, Sun C P and Nori F 2008 *Phys. Rev. A* **78** 013824
[19] Genes C, Vitali D and Tombesi P 2008 *Phys. Rev. A* **77** 050307(R)
[20] Chang Y, Shi T, Liu Y X, Sun C P and Nori F 2011 *Phys. Rev. A* **83** 063826
[21] Wilson-Rae I, Zoller P and Imamoglu A 2004 *Phys. Rev. Lett.* **92** 075507
[22] Marquardt F, Chen J P, Clerk A A and Girvin S M 2007 *Phys. Rev. Lett.* **99** 093902
[23] Genes C, Vitali D, Tombesi P, Gigan S and Aspelmeyer M 2008 *Phys. Rev. A* **77** 033804
[24] Li Y, Wu L A and Wang Z D 2011 *Phys. Rev. A* **83** 043804
[25] Agarwal G S and Huang S 2010 *Phys. Rev. A* **81** 041803
[26] Safavi-Naeini A H, Alegre T P M, Chan J, Eichenfield M, Winger M, Lin Q, Hill J T, Chang D and Painter O 2011 *Nature* **472** 69
[27] Karuza M, Biancofiore C, Bawaj M, Molinelli C, Galassi M, Natali R, Tombesi P, Giuseppe G Di and Vitali D 2013 *Phys. Rev. A* **88** 013804
[28] Xu X, *et al.* 2008 *Nat. Phys.* **4** 692
[29] Woolley M J and Clerk A A 2014 *Phys. Rev. A* **89** 063805
[30] Xu X and Taylor J M 2014 *Phys. Rev. A* **90** 043848
[31] Buchmann L F, Schreppler S, Kohler J, Spethmann N and Stamper-Kurn D M 2016 *Phys. Rev. Lett.* **117** 030801
[32] Hammerer K, Wallquist M, Genes C, Ludwig M, Marquardt F, Treutlein P, Zoller P, Ye J and Kimble H J 2009 *Phys. Rev. Lett.* **103** 063005
[33] Botter T, Brooks D W C, Schreppler S, Brahms N and Stamper-Kurn D M 2013 *Phys. Rev. Lett.* **110** 153001
[34] Bariani B, Seok H, Singh S, Vengalattore M and Meystre P 2015 *Phys. Rev. A* **92** 043817
[35] Vogell B, Kampschulte T, Rakher M T, Faber A, Treutlein P, Hammerer K and Zoller P 2015 *New J. Phys.* **17** 043044
[36] Szöke A, Daneu V, Goldhar S and Kurnit N A 1969 *Appl. Phys. Lett.* **15** 376
[37] Ghobadi R, Bahrampour A R and Simon C 2011 *Phys. Rev. A* **84** 033846
[38] Aldana S, Bruder C and Nunnenkamp A 2013 *Phys. Rev. A* **88** 043826
[39] Kanamoto R and Meystre P 2010 *Phys. Rev. Lett.* **104** 063601
[40] Yasir K A and Liu W M 2015 *Sci. Rep.* **5** 10612
[41] Dalafi A, *et al.* 2013 *J. Phys. B: At. Mol. Opt. Phys.* **46** 235502
[42] Sun Q, Hu X H, Liu W M, Xie X C and Ji A C 2011 *Phys. Rev. A* **84** 023822
[43] Zhang S, Li J, Yu R, Wang W and Wu Y 2007 *Sci. Rep.* **7** 39781
[44] Wang H, Gu X, Liu Y X, Miranowicz A and Nori F 2014 *Phys. Rev. A* **90** 023817
[45] Jiang C, Liu H, Cui Y, Li X, Chen G and Shuai X 2013 *Phys. Rev. A* **88** 055801
[46] Jiang C, Zhai Z, Cui Y and Chen G 2017 *Science China Physics, Mechanics and Astronomy* **60** 010311
[47] Chen H J, Yang J Y, Zhao D M and Wu H W 2019 *Appl. Opt.* **58** 2463
[48] Gibbs H M 1985 *Optical Bistability, Controlling Light with Light* (San Diego: Academic Press)
[49] Yosia, Ping S and Chao L 2005 *Opt. Exp.* **13** 5127
[50] Yosia, Akano Y, Tamura K, Mizumoto T and Ping S 2007 *J. Opt. Soc. Am. B* **24** 1584
[51] Marcos A P G, Hurtado A and Pereda J A M 2005 *Proc. SPIE* **5611**
[52] Jain M, Xia H, Yin Y G, Merriam A J and Harris S E 1996 *Phys. Rev. Lett.* **77** 6326
[53] Payne G M and Deng L 2003 *Phys. Rev. Lett.* **91** 123602
[54] Camacho M R, Vudyasetu K P and Howell C J 2009 *Nat. Photon.* **3** 103
[55] Glasser T R, Vogl U and Lett D P 2012 *Phys. Rev. Lett.* **108** 173902
[56] Li Y and Xiao M 1996 *Opt. Lett.* **21** 1064
[57] Deng L, Kozuma M, Hagley E W and Payne M G 2002 *Phys. Rev. Lett.* **88** 143902
[58] Sun H, Fan S L, Zhang H J and Gong Q S 2013 *Phys. Rev. B* **87** 235310
[59] Schmidt H, Campman L K, Gossard C A and Imamoglu A 1997 *Appl. Phys. Lett.* **70** 3455
[60] Huang S and Agarwal G S 2010 *Phys. Rev. A* **81** 033830
[61] Goldstein E V and Meystre P 1999 *Phys. Rev. A* **59** 3896
[62] Christ H, Search C P and Meystre P 2003 *Phys. Rev. A* **67** 063611
[63] Miyakawa T, Christ H, Search C P and Meystre P 2003 *Phys. Rev. A* **67** 063603
[64] Jiang C, Cui Y and Liu H 2013 *EPL* **104** 34004
[65] Chen H J, Wu H W, Yang J Y, Li X C, Sun Y J and Peng Y 2019 *Nanoscale Res. Lett.* **14** 73
[66] Óconnell D A, *et al.* 2010 *Nature* **464** 697
[67] Fan L, Fong K Y, Poot M and Tang H X 2015 *Nat. Commun.* **6** 5850
[68] Mahboob I, Okamoto H and Yamaguchi H 2016 *Sci. Adv.* **2** 1600236
[69] Gil-Santos E, Labousse M, Baker C, Goetschy A, Hease W, Gomez C, Lemaître A, Leo G, Ciuti C and Favero I 2017 *Phys. Rev. Lett.* **118** 063605
[70] Goto H, Lin Z and Nakamura Y 2018 *Sci. Rep.* **8** 7154
[71] Okazaki Y, Mahboob I, Onomitsu K, Sasaki S and Yamaguchi H 2016 *Nat. Commun.* **7** 11132
[72] Ma P C, Zhang J Q, Xiao Y, Feng M and Zhang Z M 2014 *Phys. Rev. A* **90** 043825
[73] Ullah K, Jing H and Saif F 2018 *Phys. Rev. A* **97** 033812
[74] Asano M, Ohta R, Yamamoto T, Okamoto H and Yamaguchi H 2018 *Appl. Phys. Lett.* **112** 201103
[75] Tavis M and Cummings F W 1968 *Phys. Rev.* **170** 379
[76] Tian L and Zoller P 2004 *Phys. Rev. Lett.* **93** 266403
[77] Holstein T and Primakoff H 1940 *Phys. Rev.* **58** 1098
[78] Boyd R W 1992 *Nonlinear Optics* (New York: Academic Press)
[79] Groblacher M S, Hammerer K and Aspelmeyer M R 2009 *Nature* **460** 724
[80] Hill J T, Safavi-Naeini A H, Chan J and Painter O 2012 *Nat. Commun.* **3** 1196
[81] Walls D F and Milburn G J 1994 *Quantum Optics* (Berlin: Springer-Verlag)
[82] Bloembergen N 1980 *J. Opt. Soc. Am.* **70** 1429